Global Distribution of Extreme Precipitation and High-Impact Landslides in 2010 Relative to Previous Years

Dalia Kirschbaum[1], Robert Adler[2], David Adler[3], Christa Peters-Lidard[1], George Huffman[4,1]

1. NASA Goddard Space Flight Center, Greenbelt, MD
2. Earth System Science Interdisciplinary Center, University of Maryland, College Park, MD
3. Science Applications International Corporation, Washington, D.C.
4. Science Systems and Applications, Inc., Lanham, MD

Corresponding Author: Dr. Dalia Kirschbaum, dalia.b.kirschbaum@nasa.gov

Abstract

It is well known that extreme or prolonged rainfall is the dominant trigger of landslides worldwide. While research has evaluated the spatiotemporal distribution of extreme rainfall and landslides at local or regional scales using *in situ* data, few studies have mapped rainfall-triggered landslide distribution globally due to the dearth of landslide data and consistent precipitation information. This study uses a newly developed Global Landslide Catalog (GLC) and a 13-year satellite-based precipitation record from TRMM data. For the first time, these two unique products provide the foundation to quantitatively evaulate the co-occurence of precipitation and landslides globally. Evaluation of the GLC indicates that 2010 had a large number of high-impact landslide events relative to previous years. This study considers how variations in extreme and prolonged satellite-based rainfall are related to the distribution of landslides over the same time scales for three active landslide areas: Central America, the Himalayan Arc, and central-eastern China. Several test statistics confirm that TRMM rainfall generally scales with the observed increase in landslide reports and fatal events for 2010 and previous years over each region. These findings suggest that the co-occurrence of satellite precipitation and landslide reports may serve as a valuable indicator for characterizing the spatiotemporal distribution of landslide-prone areas in order to establish a global rainfall-triggered landslide climatology. This study characterizes the variability of satellite precipitation data and reported landslide activity at the globaly scale in order to improve landslide cataloging, forecasting and quantify potential triggering sources at daily, monthly and yearly time scales.

1. Introduction

It is well established that intense or prolonged rainfall can trigger slope movements (Cannon and Ellen 1985; Caine 1980; Croizer 1986). These processes predominately occur within steep topography where intense or prolonged rainfall increases pore water pressures and decreases soil cohesion in the subsurface, causing the driving forces to overcome resisting forces on a hillslope and activate a landslide (Wieczorek 1996; Iverson 2000). Understanding the distribution of mass movement processes can be challenging as physically-based models require *in situ* knowledge of the surface and subsurface conditions at local scales in order to quantify how rainfall intensity and infiltration may trigger landslide events. In lieu of detailed surface information, research has relied on statistical or empirical comparisons of rainfall events and landslides to characterize the spatial and temporal distributions of mass movements at local or regional scales based on historical landslides and gauge-based rainfall (Caine 1980; Larsen and Simon 1993; Guzzetti et al. 2008; Lepore et al. 2011). A challenge inherent in both physical and empirical *in situ* evaluations is the availability of consistent precipitation information and landslide event data to effectively characterize the spatiotemporal distribution of landslide occurrences as well as validate these models, particularly over regional or global scales.

A newly developed Global Landslide Catalog (GLC) represents the first database of its kind to catalog all rapidly-moving, rainfall-triggered landslides within the recent past at the global scale (Kirschbaum et al. 2009a). The catalog currently contains five complete years of data (2003, 2007 – 2010) with continued reporting to the present. Through evaluation of this GLC dataset, we are able to extract information on the spatial and temporal frequency of landslide events at the global scale. While the GLC has several limitations identified below, the catalog provides a

foundation for exploring where and when landslide-triggering extreme storms have occurred over the globe and for characterizing hotspots for both landslides and extreme rainfall activity. We compare the GLC with satellite precipitation data from the Tropical Rainfall Measuring Mission (TRMM) Multi-Satellite Precipitation Analysis (TMPA), which offers a 13-year rainfall product at sub-daily time scales from 50°N to 50°S and spatial uniformity over most landslide-prone regions.

This study represents a first step in determining how variations in satellite precipitation are related to variations in landslides reported in the GLC, primarily on seasonal and inter-annual time scales and on regional spatial scales. Although satellite-based rainfall information has limitations in mountainous regions, the globally uniform nature of the data makes it very useful in comparison with the global landslide database. Previous research has applied remotely sensed data to evaluate magnitude-size relationships, progression and cataloging of landslides as well as to study channel morphology and contributing slope area to potential failure sources (Lashermes et al. 2007; Galewsky et al. 2006; Singhroy et al. 2002; Petley et al. 2002; Haeberlin et al. 2002). This analysis as well as previous related studies employ satellite-based rainfall estimates to evaluate landslide hazards with the goal of assessing their distribution over the global or regional scale (Hong et al. 2006; Kirschbaum et al. 2011; Liao et al. 2011). While the spatial resolution (0.25°x0.25°) of the TMPA product precludes its use for detailed hillslope investigations since precipitation can vary substantially within a single grid box, TMPA data shows promise in characterizing landslide processes over larger areas using statistical or empirical methodologies.

Upon completion of the rainfall-triggered landslide catalog for 2010[1], the authors noted significantly more high-impact landslides for 2010 compared to previous years in the record. For example, a catastrophic mudslide occurred in Zhouqu County in Gansu, China on August 8th, 2010 which killed 1,765 people and resulted in an estimated 759 million USD in damages (EM-DAT 2011). Additional damaging landslides occurred in: Bududa, Uganda in March causing nearly 400 fatalities; Leh in Ladakh, Indian Kashmir in August which resulted in an estimated 245 fatalities; and a series of events in eastern Brazil during January and April which killed over 700 people. Media reports identified intense rainfall as the trigger for each of these events, which mobilized large volumes of material and interacted with the local morphology to generate catastrophic landslides.

Drawing upon the global nature of the GLC as well as quasi-global satellite precipitation information, this research seeks to determine whether 2010 was an anomalous year for extreme precipitation and landslide activity as well as outline potential sources for this behavior. This research examines the co-occurrence of the GLC and TMPA precipitation in order to quantitatively determine how these datasets may inform each other in terms of the spatial distribution of extreme rainfall and occurrence of landslide "hotspots" over the globe. Through this evaluation, the analysis also considers how these established relationships may help to potentially forecast landslide activity and variability at seasonal, annual and decadal scales. This work may also serve as a building block to move one step closer to developing a global climatology of rainfall-triggered landslides, which currently does not exist and is greatly needed by many different organizations from international aid agencies to local governments.

[1] Landslide inventory information and documentation is available at http://trmm.gsfc.nasa.gov/publications_dir/potential_landslide.html

This paper focuses on observations of anomalous rainfall-triggered landslide reports during 2010 and considers how the landslides relate to mean monthly or daily rainfall for 2010 over three particularly active areas. The paper then considers the extent to which corresponding extreme daily or monthly rainfall signatures differ in 2010 compared to previous years in the GLC. Lastly, this study provides a discussion of the potential sources for why 2010 may represent an anomalous year over the three study areas considered as well as how this type of analysis may be expanded and applied in the future.

1.1. Data description

Landslide inventory

Few databases have attempted to catalog landslide occurrences at the global scale outside of merely listing the sources for relevant landslide articles. Petley et al. (2005) has developed a valuable global database of fatal landslide events from 2003 to the present and reports on recent significant landslides around the world on a blog site (http://blogs.agu.org/landslideblog/). The Global Landslide Catalog (GLC), developed by the authors, considers all rapidly-moving landslides (term used herein to refer to debris flows, mudslides, landslides, etc.) directly triggered by intense or prolonged rainfall (Kirschbaum et al. 2009a). Landslide event information is obtained from online media reports, disaster databases, and governmental and non-governmental organizations, as well as personal correspondence in some cases. The landslide entries include information on the date of the landslide, the location (both nominal and latitude/longitude), type of movement (if available), trigger (heavy rainfall, storm name, or any secondary triggers if reported) and impacts (fatalities, injuries or affected persons, and additional information). The GLC has been compiled since 2007 and provides a retrospective assessment

for 2003 (Kirschbaum et al. 2009a). The GLC has also been used to evaluate a real-time, quasi-global estimation of landslide events using satellite precipitation information (Kirschbaum et al. 2009b).

This inventory provides the first global picture of all available rainfall-triggered landslide reports; however, the catalog only represents a fraction of the total number of rainfall-triggered landslides occurring around the world due to several limitations. The primary challenges of this cataloging effort stem from the complex nature of landslide processes as well as the availability and accuracy of landslide reports. The catalog only includes a landslide report if rainfall was identified as the primary trigger of the event. The GLC relies on media reports and is consequently impacted by reporting issues including accuracy of the reported information and challenges in identifying the timing and location of reported events. While the inventory contains some information gleaned from non-English articles, the GLC primarily uses landslide reports in English. Landslide information and impacts are also frequently grouped with other hazards (e.g. floods, tropical cyclones), making it difficult to clearly identify the timing, location and magnitude of the specific landslide events. Lastly, it is often difficult to identify the precise location of the landslide event due to vague reporting or difficulty in locating remote villages where events have taken place. A qualitative "confidence radius" metric is included to indicate the relative confidence of each report's latitude and longitude. An additional qualitative metric is used to describe the relative size of reported landslides based on reported impacts and the areal extent affected (i.e. street, town, or larger) with the goal of discriminating between smaller and larger events.

Despite the cited challenges, the landslide catalog contains over 2,700 events with 10,500 reported fatalities for 60 different countries over the years 2007 to 2010. Fig. 1 displays the number of landslides that caused at least 1 fatality (referred to herein as fatal landslides) per country over the consecutive GLC record as well as fatal and total landslide reports by month for each year. Upon compilation and evaluation of the 2010 record, we observed a notable increase in the number of reported landslides, fatal events and fatalities, including a three-fold increase in the number of reported events and a two-fold increase in reported fatalities and fatal events as compared to previous years. In this study we consider how reported and fatal landslide events for 2010 and previous years may co-vary with extreme or prolonged rainfall in order to establish a potential indicator for more effectively characterizing landslide-prone areas at the global scale at seasonal and interannual time scales.

Rainfall Information

This research uses daily TMPA precipitation data to characterize rainfall signatures and variability that produce damaging landslides. This merged satellite-based precipitation product provides a 13-year, 3-hourly continuous record from 50°N to 50°S at 0.25° x 0.25° resolution every 3-hours. The TMPA (Version 6) rainfall analysis uses multiple satellite estimates, all calibrated or adjusted by the TRMM radar/radiometer combined estimate (TRMM product number 2B31) and also uses a monthly rain gauge analysis to adjust the bias over land areas (Huffman et al. 2007, 2010). The TMPA has been validated against daily gauges and does well at reproducing the high end of the daily rainfall distribution. It also has the advantage of uniformity over the globe. The TMPA has also been shown to be useful in flood detection when it is used to drive a hydrological model (Yilmaz et al. 2010). Although there are limitations

regarding the accuracy of satellite rainfall estimates, including merged products such as the TMPA, the daily and monthly satellite-based estimates used here should be adequate for comparison with the landslide information.

The GLC was initially developed for evaluation of a global landslide hazard forecasting algorithm, which couples a global static landslide susceptibility map with TMPA satellite-based rainfall intensity and duration information to identify potential areas of landslide activity (Hong et al. 2007; Kirschbaum et al. 2009b; Hong et al. 2006). Hong et al. (2006) calculated an empirical intensity-duration (I-D) threshold using TMPA data and a set of global landslide events to specify an average rainfall intensity threshold above which a landslide may be triggered. This study uses the global 1-day threshold value of 79 mm/day to represent potential landslide triggering due to extreme rainfall.

2. Rainfall Anomalies and 2010 Landslides

2.1 Global Distribution of Landslides

In order to characterize the relationship between extreme precipitation hotspots and landslides during 2010, we first consider whether the pronounced increase in landslide reports (either fatal or total reported events) represents an artifact of the catalog or if there are observable patterns in increased activity for 2010. Fig. 1 highlights the increase in the number of reports, fatalities and fatal events for 2010. Fig. 2 displays the distribution of reported landslides and fatal landslides, plotted by month for the years 2007-2010 for the two large regional areas (South Asia and the

Americas) that dominate the statistics. The two figures illustrate that many of the landslide reports are distributed in reasonably well-defined regional clusters.

We identify three key areas where reported landslide activity has been fairly consistent throughout the record but which exhibit a pronounced increase in reports during 2010. These regions include Central America, the Himalayan arc and central-eastern China, representing some of the most active rainfall-triggered landslide areas in the world (Fig. 2). Through this evaluation, we investigate the connection between increased reporting and anomalous rainfall activity in these regions and how that may affect the global total of landslides. These areas are chosen based on the availability of landslide inventory information; however, we feel that the test areas provide a representative cross-section of highly susceptible areas over the globe and cover diverse climatologic and topographic regimes. Landslide reports and TMPA pixels were extracted for each of these regions and compared for both extreme daily rainfall and monthly anomalies. Several other regions displaying regional maxima and minima in 2010 were evaluated but are not included in this paper because they contained a limited number of data points for other years in the record or the landslide reporting was deemed to be inconsistent. Areas evaluated include the Northwest and Appalachian range within the United States, parts of South America, the Philippines, Indonesia and Southeast Asia.

2.2 Satellite Rainfall

Fig. 3 illustrates the TMPA yearly rainfall anomaly map for 2010, using the yearly average over the evaluation period 1998-2010. Large anomalies over Burma and central Africa are primarily due to poor gauge coverage in the gauge analysis used by the TMPA in the current version (to be

corrected in the next version of this product). The climatology and anomalies of the TMPA compare favorably with exclusively gauge-based global products over the three test areas in this study. While the TMPA product has known problems over orographically complex terrain due to challenges in passive microwave rainfall retrievals, using the TMPA data allows for consistency when computing monthly totals and daily extreme precipitation statistics over different regions.

The global anomalies for 2010 show above-average rainfall over the three study areas (Central America, China, and the Himalayan arc) for 2010. However, to explore how the various time scales and rainfall intensities are related to landslides events, we examine the distribution of both monthly and extreme daily rainfall using three test metrics:

Monthly Rainfall Anomalies

The 2010 and other years' monthly rainfall totals were compared to the month climatology calculated from the TMPA 3-hr resolution record for 1998 – 2010 to obtain anomaly fields for comparison with the landslide data for 2010 and other years.

Daily threshold exceedance

The 1-day rainfall intensity value from the global I-D threshold is used as the threshold to determine how frequently extreme rainfall occurred over the test areas. Any time the daily precipitation for a given pixel exceeds 79 mm/day, it is considered a "hit." The number of "hits" are summed over the test area by month and divided by the number of total pixels in the test area to provide a relative threshold exceedance rate, which is intended to provide a comparison between extreme daily rainfall for 2010 and previous years. Exceedance rates are computed

monthly for 2010 and averaged for the years 2007 – 2009 to be consistent with the continuous GLC record. These values are compared with reported landslides over the same month for each region. The number of "hits" is also summed over each study region for each month and compared to monthly precipitation and fatal landslides.

Quantile-Quantile Plots

The third metric tests whether 2010 daily rainfall values are statistically significantly different from previous years for the upper tail of distribution for the TMPA record. Precipitation quantiles are calculated for daily rainfall for 2010 and the years 1998 – 2009 within each study area and plotted on Quantile-Quantile (Q-Q) plots to determine if the probability distributions of two samples are independent. The two time periods are considered to be from different distributions if the quantile values diverge from their joint linear distribution. Quantiles are plotted against two lines: the 1:1 line (green) has a slope of 1, and interquartile line (red) shows the linear distribution of the 25^{th} and 75^{th} quantile for both datasets (shown in Figs. 4 – 6). A steeper positive slope of the interquartile line indicates that 25^{th} and 75^{th} quantiles of the 2010 precipitation data have a larger spread (i.e. more extreme values). If the interquartile line diverges significantly from the 1:1 line, it suggests that the distributions between the two datasets (2010 vs. 12-year record) are different within the interquartile range of each dataset.

The Kolmogorov-Smirnov (K-S) test is then used to compare the probability distribution of the two datasets by calculating the distance between the cumulative distribution functions of the two samples (Massey 1951). The null hypothesis for the K-S test assumes that the two datasets come from the same continuous distribution. The null is rejected if the two datasets have different

continuous distributions at a given significance level (α) based on the K-S test statistic and p-value. The K-S test statistic is defined as the maximum difference between the two datasets' cumulative distributions and the corresponding p-value determines the probability of obtaining the given K-S test statistic. The Q-Q distribution plotting and K-S test are performed using Matlab© software. If the p-value is lower than the designated significance level, the null hypothesis is rejected. Since this research is focused on comparing only extreme daily precipitation, the K-S test is computed for precipitation values exceeding the 75th quantile of the precipitation record. Q-Q plots and K-S test statistics are calculated for each region and shown in Table 1.

3. Landslides and precipitation hotspots

3.1 Central America

The Central American test area extends from the southern tip of Mexico to Costa Rica and includes 355 TRMM (approximately 221,900 km^2) pixels and 86 landslides from 2007 – 2010 (Fig. 2a,b). The monthly climatology shows a peak in boreal summer rainfall, punctuated by a mid-summer drought (MSD) in July, consistent with previous research (Magana et al. 1999) (Fig. 4a). Tropical cyclone activity is somewhat suppressed during the MSD and picks up again in late August or September.

The 79 mm/day minimum threshold was applied for the years 2007 – 2010 to evaluate daily exceedance values; however, the global threshold proved to be too high for the daily precipitation values observed in this area, resulting in only a few days when the threshold was exceeded. Recent work has suggested that a regionally-based I-D threshold may be better equipped to identify potential landslide triggering conditions over this study area, citing a value

of 39 mm/day as a more appropriate minimum daily rainfall threshold (Guzzetti et al. 2008; Kirschbaum et al. 2011). Fig. 4b plots the rainfall threshold exceedance rate for 2010 and 2007 - 2009 using the regional threshold proposed by Guzzetti et al. (2008) along with corresponding reported landslides. The 2010 exceedance rate highlights a dual peak in extreme precipitation that nearly parallels the occurrence of landslides reported in 2010. Both the exceedance rate and reported landslide values are nearly twice as large for most of the summer months in 2010 compared to the same months in 2007 – 2009.

Fig. 4c plots the quantile values for the 12-year TMPA daily record (x-axis) and the 2010 daily precipitation values (y-axis). Table 1 provides results from the K-S test for values above 75^{th} quantile, showing a K-S test statistic of 0.1792 and p-value of 0.0026. These values suggest that the null hypothesis can be rejected at the 99.7% confidence level. From the results in Table 1 and Q-Q plot in Fig. 4c it appears that 2010 and the previous record have different distributions above the 75^{th} quantile and that the precipitation quantiles are somewhat larger for the 12-year record compared to 2010. However, because there is a significant positive difference (on the order of 3 mm or larger) between the interquartile range line (red) and the 1:1 line (green), the results indicate that the 2010 daily precipitation quantiles are actually larger when compared to the 1998 – 2009 record.

3.2 Himalayan Arc

Along the southern margin of the Himalayan mountain range, including portions of India, Nepal, and Pakistan, monsoon rains trigger large numbers of damaging and fatal landslides each year. In 2010, landslides caused approximately 500 fatalities in July through September over the study

region. The study area for this evaluation contains 700 TMPA pixels and 284 landslide reports, which covers an area of roughly 468,000 km^2 (Fig. 2c,d). Fig. 5a displays the monthly climatology for this region and shows a clear 100-150 mm higher peak in monthly precipitation during July through September for 2010 compared to the climatology. Fig. 5b plots the daily threshold exceedance rates for 2010 and 2007 – 2009 using the global 79 mm/day threshold. When exceedance rate values are compared with the reported landslides, results show that exceedance rate values were approximately 1.5 times higher than the average values from previous years for the months of July through September. The number of reported landslides shows a similar peak, with values nearly five times higher for 2010 compared to the mean of previous years, and roughly twice as high for fatal landslides over the same time period.

The Q-Q plot shown in Fig. 5c indicates that quantile values for the 2010 data diverge from the interquartile line as well as the 1:1 line after approximately 3.7 mm/day, corresponding to the 79^{th} quantile. Results from Table 1 indicate that the K-S test produces a high K-S test statistic and a very low p-value, suggesting that the null hypothesis may be rejected at the 99.9% confidence level and that the extreme precipitation values for 2010 are significantly higher than for the 1998 – 2009 TMPA record.

3.3 China

The test area within central-eastern China contains 810 TRMM pixels (approximately 512,700 km^2) and 34 landslides (Fig. 2c,d). Fig. 6a displays a pronounced peak in the 2010 monthly totals for July and August, which is consistent with the peak in landslides during the same months (Fig. 6b). The rainfall threshold exceedance rates for 2010 and 2007 – 2009 indicate that July is the

peak month for extreme daily precipitation. However, when comparing the monthly values with the landslide record, it is evident that anomalously high rainfall accumulations were observed for both July and August. The Q-Q plot shows that after approximately 8.7 mm/day (corresponding to the 95th quantile) the 2010 quantile values diverge from the 12-year distribution, suggesting that the most intense daily precipitation values were higher in 2010 compared to previous years (Fig. 6c). The K-S test for the 75th quantile and higher (corresponding to a rain rate of 2.42 mm/day) does not reject the null hypothesis. However, at the highest precipitation values (above the 90th quantile) the null is rejected with a p-value of 0.0276 at the 96% confidence level. While the climatology and highest daily precipitation values indicate that 2010 may be different from previous years, this area provides much less conclusive results. Sources of uncertainty are discussed below.

3.4 Comparison of the three test regions

Fig. 7 compares the monthly rainfall and exceedance threshold values for each month in the record over the three study areas. The 79 mm/day threshold was used for the India and China study regions and the 39 mm/day threshold was applied for Central America. Fig. 7a displays a scatter plot of monthly rainfall vs. exceedance values for each month over the study regions from 2007 – 2010, showing a clear positive linear trend between increasing monthly rainfall totals and increased number of 'hits' when the daily rainfall threshold was exceeded. Monthly rainfall (Fig.7b) and exceedance threshold values (Fig. 7c) are also compared to fatal landslides for each month. The number of fatal landslides is averaged over each 50 mm or 50 exceedance value interval. Fig. 7b and c suggest that despite having an uneven number of data points within each bin, there appears to be a slight increase in the average number of fatal landslides as the monthly rainfall or exceedance values increase.

4. Discussion

The GLC dataset provides a unique global validation proxy for evaluating co-occurrence of extreme and prolonged rainfall and high-impact landslide events. Within this evaluation, we identify 2010 as an active year for rainfall-triggered landslides at the global scale and relate precipitation signatures to the GLC in order to determine how inter-annual precipitation variations are related to variations in landslides within the three identified landslide-prone regions. While it is well-known that intense or prolonged precipitation and landslide initiation processes are linked, the global nature of the GLC and TMPA precipitation record allows us to quantitatively diagnose this relationship at regional and global scales for the first time. Establishing direct correlations between these two products in terms of how they co-vary over space and time is complicated due to incomplete data records. This work will continue to improve upon the existing GLC in order to amass a more robust record of landslide events and accurately link rainfall patterns with landslide triggering events.

From this analysis, we determine that there is a clearly observable increase in rainfall-triggered landslide reports during 2010, compared to previous years. Fig. 1b and c displays the monthly distribution of fatal and total reported landslide for the years 2007 to 2010. The increased peak in fatal reports during August corresponds to a large peak in activity from monsoon rains, with approximately 60% of the fatal reports occurring in China, Nepal and India alone. The total number of landslide reports is on the order of three times larger than the previous years' inventory. In addition to the increase in anomalous rainfall-triggered events observed over the three study regions in 2010, the increased number of events may also partially be a result of improved reporting and better cataloging of reports. One way to consider a more realistic global

distribution of landslide activity is to only consider fatal reports, a potentially more reliable statistic since fatal events are generally more likely to be reported. Despite the short record, we have observed an increase in the number of fatal landslides over the lifetime of the inventory, which is consistent with Dr. Petley's findings for fatal landslides for 2003 to 2010 and shows a peak in fatal landslides for 2010 (Petley 2011). While variability in reporting accuracy is extremely challenging to characterize between regions, we anticipate that as we have more years of landslide report data we may be able to classify geographic biases in the GLC.

The precipitation anomalies shown in Fig. 3 highlight several areas that have experienced particularly wet seasons in 2010, including the three study areas evaluated here as well as southern India, Indonesia, eastern Australia, and northwestern South America. Within these areas, Indonesia, and portions of Colombia, Venezuela and Brazil in South America also experienced increases in landslide activity with more fatal landslide reports. Comparatively, in countries with negative precipitation anomalies such as Vietnam, we observed fewer reported landslide events.

There are many driving factors influencing regional variations in rainfall accumulation and intensity on seasonal and annual scales. The El Niño/Southern Oscillation (ENSO), while global in nature, has highly variable impacts on precipitation accumulation at regional scales (Ropelewski and Halpert 1987; Curtis and Adler 2003). The Nino 3, 3.4 and 4 indices show a large positive anomaly in January and February 2010, suggesting a strong El Niño (NOAA 2011). El Niño conditions continued until late February when the ENSO indices indicated a transition into La Niña conditions beginning in July and peaking in the mid to late fall, 2010.

Within the United States, wet weather likely amplified by El Niño and La Niña conditions and contributed to an increased number of landslide reports in southern California in January and February and California and Washington in December. While the El Niño signal was strongest at the beginning and the La Niña signal was strongest at the end of 2010, the majority of the rainfall events associated with anomalously high landslide activity over the study regions occurred in the boreal summer months, coinciding with a fairly weak ENSO signal. Below we discuss the impact of ENSO signals within the three study regions and their possible delayed impacts on boreal summer precipitation.

Central America

The 2010 values during the summer months show a 50 – 100 mm increase in accumulation compared to the 12-year climatology, with the largest peak in August and September over this region. The landslide reports show a similar peak in reporting during May, August – September, and November for 2010 (Fig. 4b), with three times more fatal landslides and over four times more total reports. The extreme daily rainfall quantiles and monthly accumulations all suggest that the increase in reports tends to mirror the observed anomalous precipitation in the TMPA record. The peak in reports during May and November were likely the result of two tropical cyclones: tropical cyclone Agatha on May 29-30th caused approximately 9 fatal landslides in Guatemala, and tropical storm Tomas in early November caused 2 fatal landslides in Costa Rica and many other landslide reports along roads. Due to the extreme nature of these events, there may also have been an over-reporting bias for these storms.

One of the reasons for the positive precipitation anomalies over this region could result from a fairly active 2010 tropical cyclone season in the tropical Atlantic. ENSO has been shown to modulate interannual tropical cyclone frequency and redistribute precipitation extremes(Elsner et al. 1999; Curtis et al. 2007). Curtis (2002) found that during the summer *before* a La Niña event, such was the case for 2010, precipitation follows a similar pattern to El Niño or Neutral patterns at the beginning of the summer, but then increases considerably in September. This inter-annual pattern can be linked to sea surface temperature changes and moisture due to ENSO as well as enhanced tropical cyclone activity.

Himalayan Arc

Monthly and extreme precipitation signals for the Himalayan Arc study area point to increased precipitation totals during the summer monsoon months in 2010, with the null hypothesis being rejected at the 99.9% confidence level and the exceedance values indicating a nearly two-fold increase in the number of extreme precipitation days during 2010 compared to the 2007-2009 period (Fig. 5). Several studies have evaluated the connection between monsoon rains and landslide susceptibility over this region (Nagarajan et al. 2000; Gabet et al. 2004; Petley et al. 2007). Indian Monsoon rainfall has been shown to strongly correlate with ENSO phases due to the coupling of tropical ocean-atmospheric modes over the Indian Ocean (Krishnamurthy and Goswami 2000). While Indian monsoon conditions are often suppressed during an El Niño event (Krishna Kumar et al. 2006; Webster et al. 1998), in the summer following a strong El Niño event, there is a tendency for above-normal precipitation with the most pronounced signal in August and September (Park et al. 2010). While ENSO is not the only circulation pattern contributing to the variability of boreal summer rainfall, results indicate that the strong ENSO

signal during 2010 may have played a sizeable role in the positive precipitation anomalies observed over this region.

China

Results from Fig. 6 show that there is a pronounced peak in monthly rainfall during July and August, corresponding to an increased number of landslide reports. However, both exceedance values and rainfall quantiles do not clearly show the relationship between precipitation extremes and landslide reporting. The inconsistency in the landslide reporting as well as the size of the study area may be the limiting factors in this evaluation since only 34 landslides were reported over a very large area (512,700 km^2) during the four year period. This is likely an underestimation of the GLC, due to reporting or language barriers, the occurrence of landslides in remote areas, or the influence of other triggers (such as the Wenchuan earthquake in 2008). In addition, triggers such as antecedent moisture or short, intense rainfall events (less than 24 hours), such as what caused the Zhouqu mudslide, were either not included in the database or not adequately resolved by the satellite information.

Evaluating the sources of seasonal and annual variability of summer precipitation over China is challenging due to diverse climate zones and multiple ocean-atmosphere feedbacks influencing precipitation in this region. The Asian monsoon has been shown to strongly couple with tropical SSTs and the propagation of atmospheric circulation over the western Pacific, which affects the modulation of the Asian monsoon (Yang and Lau 2004). Directly north of the China study area, Feng and Hu (2004) one study also found that during a strong ENSO, there is a coupled relationship between the Indian summer monsoon and precipitation variability over northern

China. The strength of the precipitation-landslide signal in this region is complicated by a number of factors, including a limited number of landslide reports available over this region with varied reporting accuracy, the large size of the study area considered, and additional triggers influencing landslide susceptibility and triggering including anthropogenic impacts such as population density, road construction, and mining.

Each of the study areas is impacted by a different set of regional atmospheric circulation patterns, annual rainfall totals and surface susceptibility characteristics. Figs. 2, 4 – 7 and Table 1 suggest that within the three regions, there is a statistically significant positive anomaly in 2010 when comparing landslide reports and rainfall signatures within the TMPA record. It is clear from the analysis of these test areas that the total increase of 2010 landslides globally is related to changes in precipitation over different areas. However, the causes of these precipitation anomalies associated with increases in landslides vary from region to region. There is no singular reason for the precipitation increases and the related landslide maximum in 2010.

This analysis is a first step and should be considered preliminary for a number of reasons. First, because this evaluation only considers four years of data, identify temporal signals in landslide reporting may produce erroneous results over some regions. The increase in landslide reports over the period of record is observed by another database (Petley 2011), suggesting that the a signal exists despite regional heterogeneities. As this rainfall-triggered landslide inventory continues to increase, it will provide more information to better quantify the regional reporting biases inherent in this type of a catalog.

Second, merged satellite products offer a unique perspective on rainfall distribution by providing an inter-comparison framework amongst regions and through time. However, the sampling frequency of current microwave sensors does not allow for continuous monitoring of precipitation features and as a result, short events or peak intensities may not be accurately resolved by space-borne instruments or merged data sets. Comparing TMPA with the gauge-based products indicates that both products adequately highlight regional precipitation anomalies, but may not always resolve the exact magnitude of precipitation intensity. Comparing the relative magnitude of cumulative or daily exceedance values amongst regions allows for more consistent evaluation of the global prototype landslide algorithm system and evaluation of the rainfall-landslide relationship. This underscores the motivation for identifying an observable connection between the GLC and TMPA data so as to develop a potential indicator for high-intensity rainfall, particularly over mountainous regions where existing products may have difficulty accurately resolving precipitation.

Third, antecedent moisture may also play a sizeable role in the initiation and distribution of landslide events. Moisture within the soil can cause a buildup of pore water pressure such that smaller rainfall events occurring when the soil is already saturated could trigger a mass movement. Studies have established relationships between antecedent precipitation and rainfall intensity thresholds for several different geographic regions (Glade et al. 2000; Godt et al. 2006; Chleborad et al. 2006). Moving forward, this research will consider the joint relationship between antecedent precipitation and precipitation intensity to better characterize potentially susceptible regions based on weekly, monthly or seasonal precipitation accumulation.

Fig. 7 attempts to summarize the rainfall-landslide relationships over the three test areas. The top panel indicates that monthly rainfall is fairly well correlated with the exceedance index based on daily rainfall for the three test areas. Although one would think that extreme daily rainfall would be more closely associated with landslides, it is clear that the two rainfall statistics are related. The middle and bottom panels show that both the monthly rainfall and exceedance index are correlated to landslides, but that there is significant noise. In very approximate terms, a doubling of monthly rainfall from 150 to 300 mm is related to a fatal landslide increase of about a factor of three. A similar or slightly larger increase in fatal landslides is associated with a doubling of the exceedance index. These results are only indicative of areas that are already prone to landslides. Despite the data challenges intrinsic to this empirical approach, results shown here suggest that the GLC is very useful in estimating rainfall-landslide relations both in particular regions and even integrated over the globe. The data products evaluated here represent a very noisy process, particularly when evaluated across the globe. Despite this fact, we anticipate that if this evaluation were expanded to other study areas with sufficient numbers of landslide events, we may observe a more robust relationship between landslide reports and precipitation signals.

5. Conclusions

One of the unique aspects of the GLC is that it provides the first openly available, global picture of rainfall-triggered landslides over multiple years that can be compared with global precipitation estimates. Through the use of this catalog, the distribution and frequency of landslides and fatal landslides can be compared to distributions of satellite rainfall to better quantify these relationships. This analysis also allows us to evaluate the co-occurrence of extreme precipitation and landslide “hotspots” at large spatial scales and determine how landslide variations are related to meteorological changes. From analysis of the 2010 precipitation signatures over the three

study areas, it is clear that an observable signal exists between increases in reported and fatal landslide activity and increases in precipitation accumulation and daily intensity. It is not clear from the analyses and associated statistics that daily rainfall exceedance values are a better indicator of increased landslides than just simply the anomaly in monthly rainfall. The relative importance of daily extremes vs. monthly anomalies should be examined more thoroughly with additional data as the landslide catalog increases in length. Future analyses should also take into account regional or local differences in surface characteristics, such as are contained in landslide susceptibility indexes (e.g. Nadim et al. 2006; Guzzetti et al. 2005; Lepore et al. 2011). While other factors can modify this relationship including anthropogenic modification and tectonic weakening of hillslopes among others, understanding the relative distribution of extreme precipitation may help to shed new light on potential landslide activity at daily, monthly and yearly scales. We plan to re-evaluate these changes once we have built a larger record of reported events.

Through the type of study shown here, we may be able to better characterize the relative relationship between precipitation activity and potential landslide triggering and identify where landslides may impact populations based on natural variability in seasonal precipitation from teleconnections such as ENSO. Projections of precipitation intensity and distribution in a warmer world suggest that despite model uncertainties, rainfall in many of the monsoonal regions and tropical cyclone areas will likely become more extreme (IPCC 2007). One future direction of this study is to establish more concrete global relationships between extreme precipitation and landslide activity in order to better understand how landslide disasters may be modulated under climate change conditions. New satellite missions such as the Global Precipitation Measurement

(GPM) mission (www.gpm.nasa.gov) will also help to improve spatiotemporal coverage of precipitation measurements, enabling an extended record of satellite precipitation in order to better characterize the seasonal, yearly and decadal variability of extreme precipitation and its impact on landslide activity at the global scale.

Acknowledgements

The authors acknowledge the individuals who helped to develop the GLC, including Stephanie Hill, Lynne Shupp, Teddy Allen, Pradeep Adhikari, Lauren Redmond, David Adler, and Kimberly Rodgers. This work was supported by the Global Precipitation Measurement (GPM) mission and NASA's Applied Sciences Program. Thank you also to Yudong Tian, who helped to provide TMPA data for this analysis.

References

Caine, N., 1980: The Rainfall Intensity: Duration Control of Shallow Landslides and Debris Flows. *Geografiska Annaler, Physical Geography*, **62**, 23–27.

Cannon, S. H., and S. D. Ellen, 1985: Rainfall conditions for abundant debris avalanches, San Francisco Bay region, California. *California Geology*, **38**, 12267–12272.

Chleborad, A. F., R. L. Baum, and J. W. Godt, 2006: Rainfall Thresholds for Forecasting Landslides in the Seattle, Washington, Area—Exceedance and Probability. *U.S. Geological Survey Open-File Report*, **2006-1064**.

Croizer, M. J., 1986: *Landslides: Causes, Consequences and Environment*. Croom Helm, London,.

Curtis, S., 2002: Interannual variability of the bimodal distribution of summertime rainfall over Central America and tropical storm activity in the far-eastern Pacific. *Climate Research*, **22**, 141–146, doi:10.3354/cr022141.

Curtis, S., and R. F. Adler, 2003: Evolution of El Niño-precipitation relationships from satellites and gauges. *Journal of Geophysical Research - Atmospheres*, **108**, 1–8, doi:10.1029/2002JD002690.

Curtis, S., A. Salahuddin, R. F. Adler, G. J. Huffman, G. Gu, and Y. Hong, 2007: Precipitation Extremes Estimated by GPCP and TRMM: ENSO Relationships. *Journal of Hydrometeorology*, **8**, 678–689, doi:10.1175/JHM601.1.

EM-DAT, 2011: The OFDA/CRED International Disaster Database. *Université Catholique de Louvain*,. www.em-dat.net.

Elsner, J. B., A. B. Kara, and M. A. Owens, 1999: Fluctuations in North Atlantic Hurricane Frequency. *Journal of Climate*, **12**, 427–437.

Feng, S., and Q. Hu, 2004: Variations in the Teleconnection of ENSO and Summer Rainfall in Northern China: A Role of the Indian Summer Monsoon*. *Journal of Climate*, **17**, 4871–4881, doi:10.1175/JCLI-3245.1.

Gabet, E. J., D. W. Burbank, J. K. Putkonen, B. A. Pratt-sitaula, and T. Ojhac, 2004: Rainfall thresholds for landsliding in the Himalayas of Nepal. *Geomorphology*, **63**, 131–143.

Galewsky, J., C. P. Stark, S. Dadson, C.-C. Wu, A. H. Sobel, and M.-J. Horng, 2006: Tropical cyclone triggering of sediment discharge in Taiwan. *Journal of Geophysical Research*, **111**, 1–16, doi:10.1029/2005JF000428.

Glade, T., M. Crozier, and P. Smith, 2000: Applying probability determination to refine landslide-triggering rainfall thresholds using empirical "'Antecedent Daily Rainfall Model'." *Pure and Applied Geophysics*, **157**, 1059–1079.

Godt, J. W., R. L. Baum, and A. F. Chleborad, 2006: Rainfall characteristics for shallow landsliding in Seattle, Washington, USA. *Earth Surface Processes and Landforms*, **31**, 97–110, doi:10.1002/esp.1237.

Guzzetti, F., P. Reichenbach, M. Cardinali, M. Galli, and F. Ardizzone, 2005: Probabilistic landslide hazard assessment at the basin scale. *Geomorphology*, **72**, 272–299.

Guzzetti, F., S. Peruccacci, M. Rossi, and C. P. Stark, 2008: The rainfall intensity–duration control of shallow landslides and debris flows: an update. *Landslides*, **5**, 3–17, doi:10.1007/s10346-007-0112-1.

Haeberlin, Y., P. Turberg, A. Retiere, O. Senegas, and A. Parriaux, 2002: Validation of SPOT-5 satellite imagery for geological hazard identification and risk assessment for landslides, mud and debris flows in Matagalpa, Nicaragua.

Hong, Y., R. Adler, and G. Huffman, 2006: Evaluation of the potential of NASA multi-satellite precipitation analysis in global landslide hazard assessment. *Geophysical Research Letters*, **33**, 1–5, doi:10.1029/2006GL028010.

Hong, Y., R. Adler, and G. Huffman, 2007: Use of satellite remote sensing data in the mapping of global landslide susceptibility. *Natural Hazards*, **43**, 245–256, doi:10.1007/s11069-006-9104-z.

Huffman, G. J. and Coauthors, 2007: The TRMM Multisatellite Precipitation Analysis (TMPA): Quasi-Global, Multiyear, Combined-Sensor Precipitation Estimates at Fine Scales. *Journal of Hydrometeorology*, **8**, 38–55, doi:10.1175/JHM560.1.

Huffman, G. J., R. F. Adler, D. T. Bolvin, and E. J. Nelkin, 2010: The TRMM Multi-satellite Precipitation Analysis (TMPA). *Satellite Rainfall Applications for Surface Hydrology*, Eds. F. Hossain and M. Gebremichael, 3–22, Springer Verlag.

IPCC, 2007: *Climate Change 2007: Working Group I: The Physical Science Basis*. IPCC Fourt. Eds. S. Solomon, D. Qin, M. Manning, Z. Chen, M. Marquis, K.B. Averyt, M. Tignor, and H.L. Miller. Cambridge University Press, Cambridge and New York, http://www.ipcc.ch/publications_and_data/ar4/wg1/en/contents.html.

Iverson, R. M., 2000: Landslide triggering by rain infiltration. *Water Resources Research*, **36**, 1897–1910.

Kirschbaum, D. B., R. Adler, Y. Hong, S. Hill, and A. Lerner-Lam, 2009a: A global landslide catalog for hazard applications: method, results, and limitations. *Natural Hazards*, **52**, 561–575, doi:10.1007/s11069-009-9401-4.

Kirschbaum, D. B., R. Adler, Y. Hong, and A. Lerner-Lam, 2009b: Evaluation of a preliminary satellite-based landslide hazard algorithm using global landslide inventories. *Natural Hazards And Earth System Sciences*, **9**, 673–686.

Kirschbaum, D. B., R. Adler, Y. Hong, S. Kumar, C. Peters-Lidard, and A. Lerner-Lam, 2011: Advances in landslide nowcasting: evaluation of a global and regional modeling approach. *Environmental Earth Sciences*, doi:10.1007/s12665-011-0990-3.

Krishna Kumar, K., B. Rajagopalan, M. Hoerling, G. Bates, and M. Cane, 2006: Unraveling the mystery of Indian monsoon failure during El Niño . *Science*, **314**, 115–119, doi:10.1126/science.1131152.

Krishnamurthy, V., and B. N. Goswami, 2000: Indian Monsoon–ENSO Relationship on Interdecadal Timescale. *Journal of Climate*, **13**, 579–595, doi:10.1175/1520-0442(2000)013<0579:IMEROI>2.0.CO;2.

Larsen, M. C., and A. Simon, 1993: A Rainfall Intensity-Duration Threshold for Landslides in a Humid-Tropical Environment, Puerto Rico. *Geografiska Annaler, Physical Geography*, **75**, 13–23.

Lashermes, B., E. Foufoula-Georgiou, and W. E. Dietrich, 2007: Channel network extraction from high resolution topography using wavelets. *Geophysical Research Letters*, **34**, 1–6, doi:10.1029/2007GL031140.

Lepore, C., S. Kamal, P. Shanahan, and R. L. Bras, 2011: Rainfall-induced landslide susceptibility zonation of Puerto Rico. *Environmental Earth Sciences*, doi:10.1007/s12665-011-0976-1.

Liao, Z., Y. Hong, D. Kirschbaum, and C. Liu, 2011: Assessment of shallow landslides from Hurricane Mitch in central America using a physically based model. *Environmental Earth Sciences*, doi:10.1007/s12665-011-0997-9.

Magana, V., J. A. Amador, and S. Medina, 1999: The Midsummer Drought over Mexico and Central America. *Journal of Climate*, **12**, 1577–1588.

Massey, F., 1951: The Kolmogorov-Smirnov Test for Goodness of Fit. *Journal of the American Statistical Association*, **46**, 68–78.

NOAA, 2011: Climate Prediction Center. *National Weather Service*,. http://www.cpc.ncep.noaa.gov (Accessed March 5, 2011).

Nadim, F., O. Kjekstad, P. Peduzzi, C. Herold, and C. Jaedicke, 2006: Global landslide and avalanche hotspots. *Landslides*, **3**, 159–173, doi:10.1007/s10346-006-0036-1.

Nagarajan, R., A. Roy, R. V. Kumar, A. Mukherjee, and M. Khire, 2000: Landslide hazard susceptibility mapping based on terrain and climatic factors for tropical monsoon regions. *Bull Eng Geol Env*, **58**, 275–287.

Park, H.-S., J. C. H. Chiang, B. R. Lintner, and G. J. Zhang, 2010: The Delayed Effect of Major El Niño Events on Indian Monsoon Rainfall. *Journal of Climate*, **23**, 932–946, doi:10.1175/2009JCLI2916.1.

Petley, D. N., 2011: The Landslide Blog. *AGU Blogosphere*,. http://blogs.agu.org/landslideblog/ (Accessed December 27, 2011).

Petley, D. N., W. D. O. Crick, and A. B. Hart, 2002: The use of satellite imagery in landslide studies in high mountain areas. *The Proceedings of the 23rd Asian Conference on Remote Sensing (ACRS 2002)*, Kathmandu www.gisdevelopment.net/aars/acrs/2002/hdm/48.pdf.

Petley, D. N., S. A. Dunning, and N. J. Rosser, 2005: The analysis of global landslide risk through the creation of a database of worldwide landslide fatalities. *Landslide Risk Management*, Eds. O. Hungr, R. Fell, R. Counture, and E. Ebergardt, 367–374, Balkema, Amsterdam.

Petley, D. N., G. J. Hearn, A. Hart, N. J. Rosser, S. A. Dunning, K. Oven, and W. A. Mitchell, 2007: Trends in landslide occurrence in Nepal. *Natural Hazards*, **43**, 23–44, doi:10.1007/s11069-006-9100-3.

Ropelewski, C., and M. Halpert, 1987: Global and Regional Scale Precipitation Patterns Associated with the El Nino/Southern Oscillation. *Monthly Weather Review*, **115**, 1606–1626.

Singhroy, V., K. Molch, and M. Bulmer, 2002: Characterization of landslide deposits using SAR Images. *IGARSS 2002, IEEE International Geoscience and Remote Sensing Symposium and the 24th Canadian Symposium on Remote Sensing*, Vol. 00 of, 185–187.

Webster, P. J., V. O. Magana, T. N. Palmer, J. Shukla, R. A. Tomas, M. Yanai, and T. Yasunari, 1998: Monsoons : Processes , predictability , and the prospects for prediction 2 . Description of the Monsoons. *Journal of Geophysical Research*, **103**.

Wieczorek, G. F., 1996: Landslide Triggering Mechanisms. *Landslides: Investigations and Mitigation*, Eds. K.A. Turner and R.L. Schuster, 76–88, Transportation Research Board, Washington, D.C.

Yang, F., and K.-M. Lau, 2004: Trend and variability of China precipitation in spring and summer: linkage to sea-surface temperatures. *International Journal of Climatology*, **24**, 1625–1644, doi:10.1002/joc.1094.

Yilmaz, K. K., R. F. Adler, Y. Tian, Y. Hong, and H. F. Pierce, 2010: Evaluation of a satellite-based global flood monitoring system. *International Journal of Remote Sensing*, **31**, 3763–3782, doi:10.1080/01431161.2010.483489.

Figure Captions

Fig. 1: Distribution of GLC for 2007 – 2010, highlighting: a) the distribution of total fatal landslides by country over the record with individual event locations for all reported landslides shown for 2010; and monthly distribution of b) fatal landslides and c) all reported landslides shown by year.

Fig. 2: Distribution of landslide reports for the years 2007 – 2010, showing a) reported and b) fatal landslides in North and South America, and c) reported and d) fatal landslides in Asia and Oceania. The boxes denote the three study areas evaluated in this paper: Central America, Himalayan Arc, and central-eastern China. Circles denote landslides for 2010, + signs display other years. The color denotes their moth of occurrence.

Fig. 3: 2010 daily precipitation anomalies computed from a TMPA daily climatology for 1998 – 2010 in mm/day. Blue (positive) areas indicate regions with higher daily precipitation totals, orange (negative) areas display dryer conditions for 2010.

Fig. 4: Precipitation analysis results for Central America study area, showing: a) Monthly rainfall accumulation for 2010 (red) with 12-year monthly climatology (green) calculated from the TPMA record (1998-2009); b) normalized threshold exceedance values (using the regional 39 mm/day threshold) summed for each month in 2010 (red) and average values for 2007 – 2009 (blue) compared to the landslide occurrence for 2010 and average number of reports from 2007 – 2009; c) Q-Q plot showing the distribution of quantiles for the 12-year TMPA record (x-axis) vs. the 2010 daily values (y-axis). The interquartile line (red) and 1:1 line (green) provide a

reference to compare the distributions of quantiles for both periods. Evaluation statistics are shown in Table 1.

Fig. 5: Precipitation analysis results for Himalayan study area, showing: a) monthly climatology comparing 2010 (red) with 12-year climatology (green); b) normalized threshold exceedance values using the globally 79 mm/day threshold for 2010 and 2007 – 2009 with reported landslide events; c) Q-Q plot showing the distribution of quantiles for the 12-year TMPA record (x-axis) vs. the 2010 daily values (y-axis), compared against the 1:1 line (green) and interquartile line.

Fig. 6: Precipitation analysis results for the China study area, showing: a) monthly climatology comparing 2010 (red) with 12-year climatology (green); b) normalized threshold exceedance using the globally 79 mm/day threshold compared to landslides over the same periods; c) Q-Q plot showing the distribution of precipitation quantiles for the 12-year TMPA record (x-axis) vs. the 2010 daily values (y-axis).

Fig. 7: Scatter plots showing the monthly values for 2007 – 2010, comparing monthly precipitation and summed threshold exceedance pixels over each of the study areas with fatal landslides for each corresponding month over the 4 year record. The Central American region uses the 39 mm/day regional threshold (Guzzetti et al. 2008), while the Himalaya and China regions both use the 79 mm/day global threshold. Filled in symbols denote 2010 months. The three plots show: a) monthly rainfall (x-axis) vs. the sum of the exceedance values (y-axis); b) monthly rainfall (x-axis) vs. fatal landslides for each month (y-axis), showing the mean number of fatal landslides for each 50 mm; c) sum of exceedance values over each area (x-axis) vs. fatal

landslides (y-axis), showing the mean number of fatal landslides plotted at an interval of 50 "hits" of the exceedance threshold.

Table 1: Test statistics for the 3 study areas, showing the 75th quantile, K-S test statistic and p-value, if the null was rejected, and the confidence level for rejecting the null.

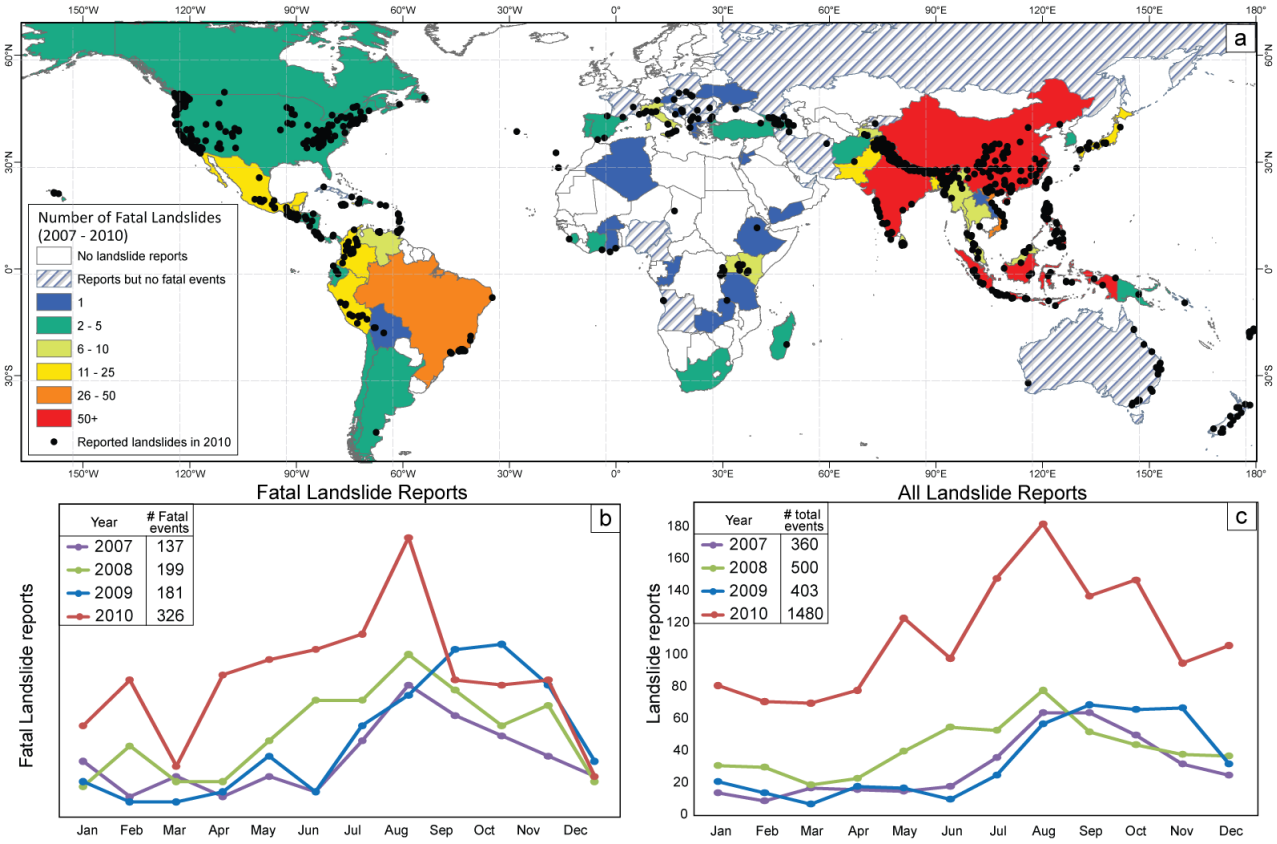

Fig. 1: Distribution of GLC for 2007 – 2010, highlighting: a) the distribution of total fatal landslides by country over the record with individual event locations for all reported landslides shown for 2010; and monthly distribution of b) fatal landslides and c) all reported landslides shown by year.

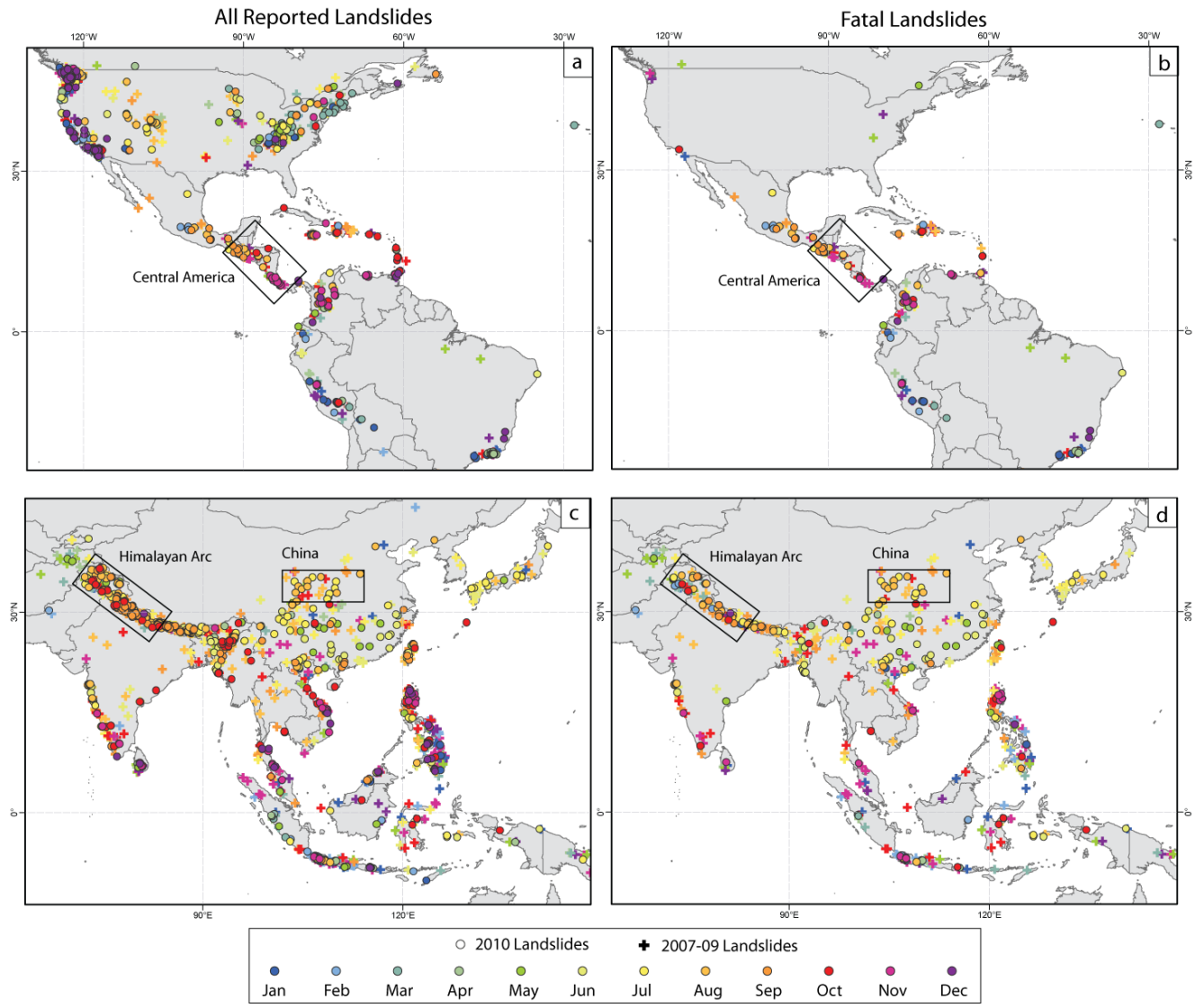

Fig. 2: Distribution of landslide reports for the years 2007 – 2010, showing a) reported and b) fatal landslides in North and South America, and c) reported and d) fatal landslides in Asia and Oceania. The boxes denote the three study areas evaluated in this paper: Central America, Himalayan Arc, and central-eastern China. Circles denote landslides for 2010, + signs display other years. The color denotes their moth of occurrence.

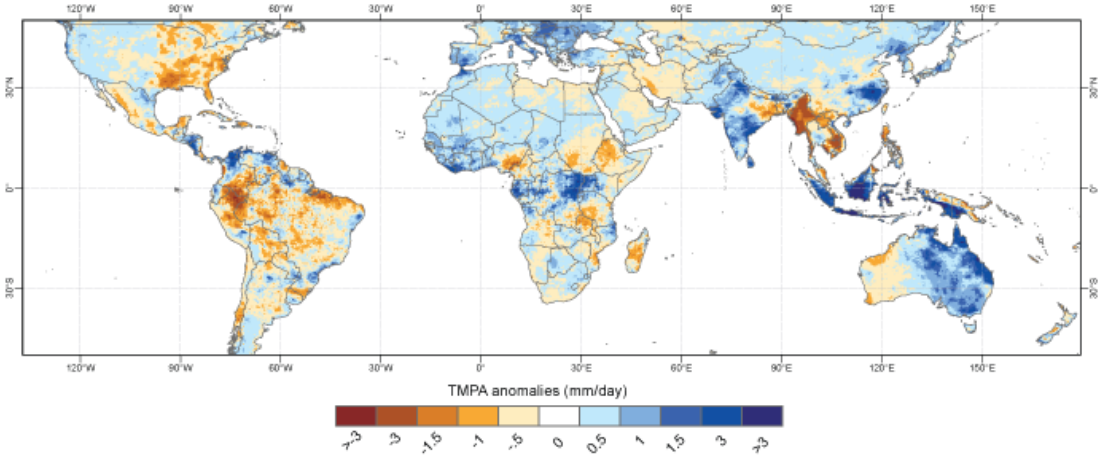

Fig. 3: 2010 daily precipitation anomalies computed from a TMPA daily climatology for 1998 – 2010 in mm/day. Blue (positive) areas indicate regions with higher daily precipitation totals.

orange (negative) areas display dryer conditions for 2010.

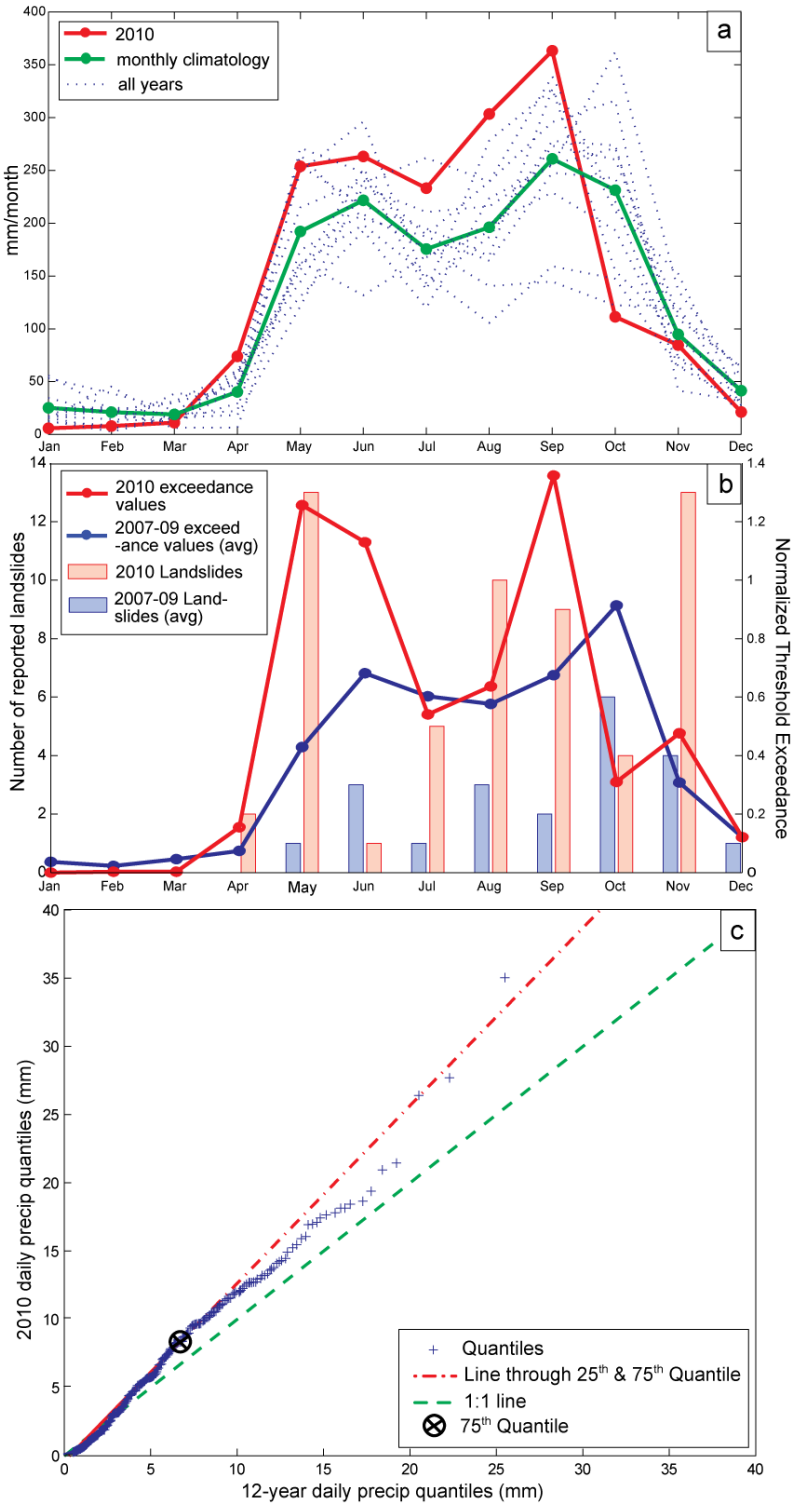

Fig. 4: Precipitation analysis results for Central America study area, showing: a) Monthly rainfall accumulation for 2010 (red) with 12-year monthly climatology (green) calculated from

the TPMA record (1998-2009); b) normalized threshold exceedance values (using the regional 39 mm/day threshold) summed for each month in 2010 (red) and average values for 2007 – 2009 (blue) compared to the landslide occurrence for 2010 and average number of reports from 2007 – 2009; c) Q-Q plot showing the distribution of quantiles for the 12-year TMPA record (x-axis) vs. the 2010 daily values (y-axis). The interquartile line (red) and 1:1 line (green) provide a reference to compare the distributions of quantiles for both periods. Evaluation statistics are shown in Table 1.

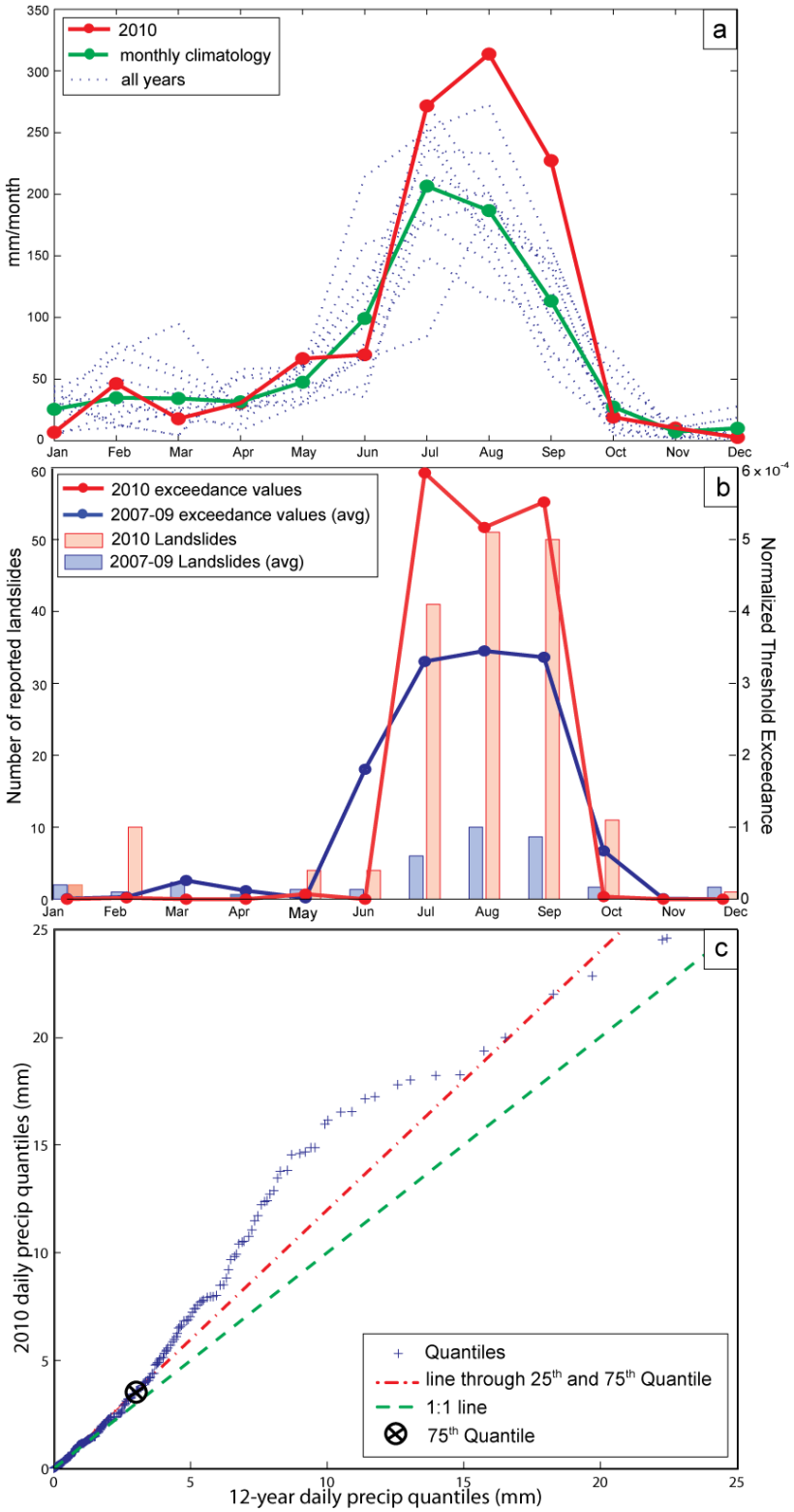

Fig. 5: Precipitation analysis results for Himalayan study area, showing: a) monthly climatology comparing 2010 (red) with 12-year climatology (green); b) normalized threshold exceedance

values using the globally 79 mm/day threshold for 2010 and 2007 – 2009 with reported landslide events; c) Q-Q plot showing the distribution of quantiles for the 12-year TMPA record (x-axis) vs. the 2010 daily values (y-axis), compared against the 1:1 line (green) and interquartile line.

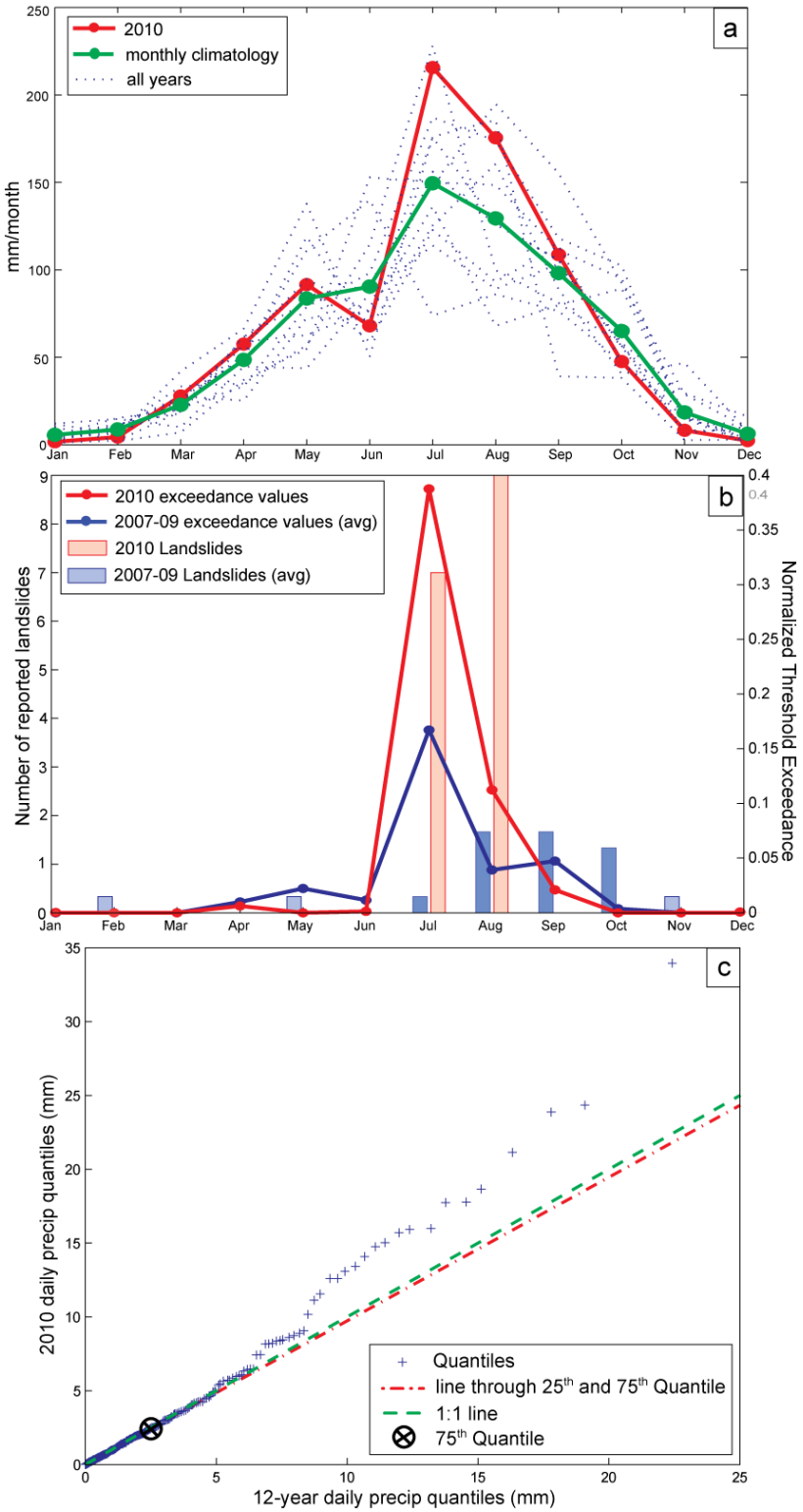

Fig. 6: Precipitation analysis results for the China study area, showing: a) monthly climatology comparing 2010 (red) with 12-year climatology (green); b) normalized threshold exceedance using the globally 79 mm/day threshold compared to landslides over the same periods; c) Q-Q

plot showing the distribution of precipitation quantiles for the 12-year TMPA record (x-axis) vs. the 2010 daily values (y-axis).

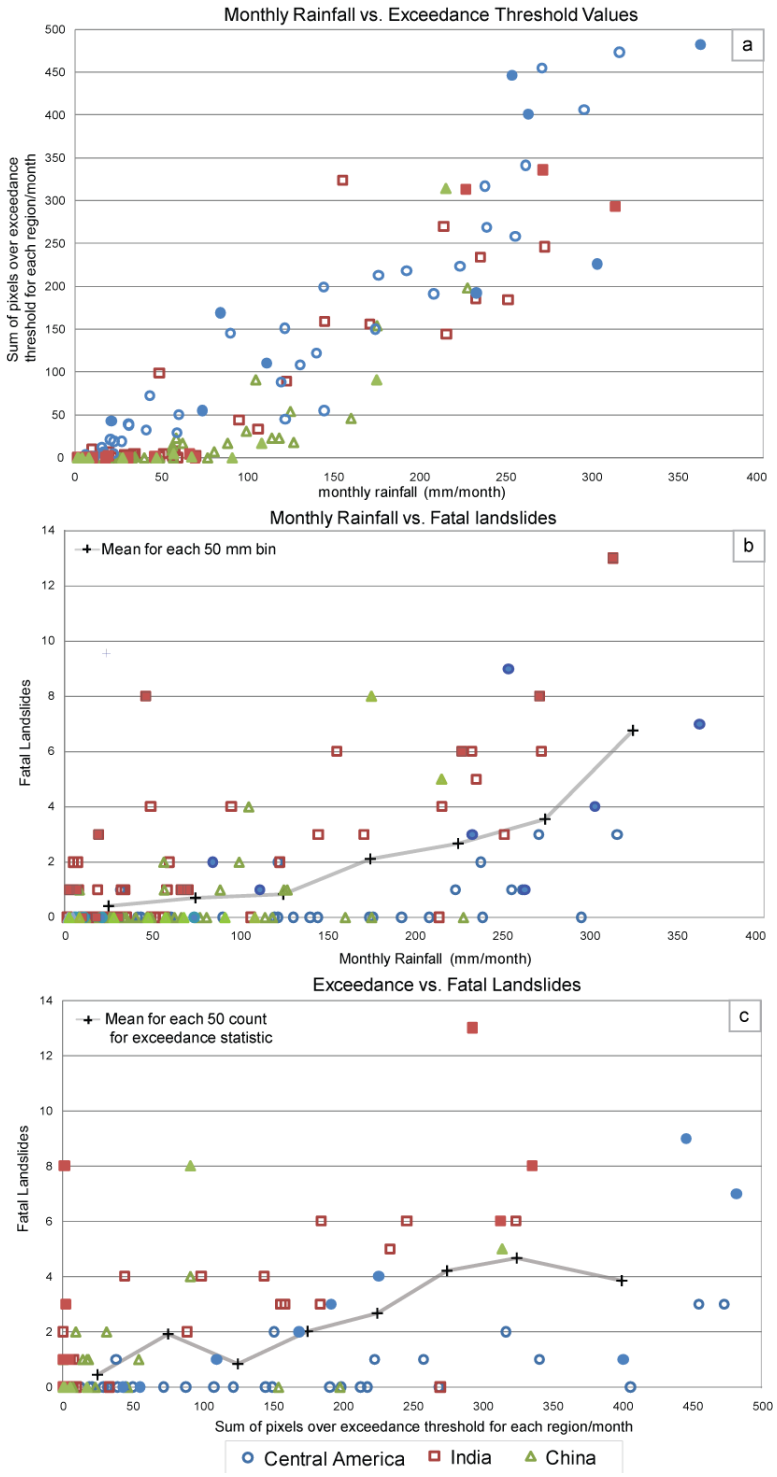

Fig. 7: Scatter plots showing the monthly values for 2007 – 2010, comparing monthly precipitation and summed threshold exceedance pixels over each of the study areas with fatal landslides for each corresponding month over the 4 year record. The Central American region uses the 39 mm/day regional threshold (Guzzetti et al. 2008), while the Himalaya and China regions both use the 79 mm/day global threshold. Filled in symbols denote 2010 months. The three plots show: a) monthly rainfall (x-axis) vs. the sum of the exceedance values (y-axis); b) monthly rainfall (x-axis) vs. fatal landslides for each month (y-axis), showing the mean number of fatal landslides for each 50 mm; c) sum of exceedance values over each area (x-axis) vs. fatal landslides (y-axis), showing the mean number of fatal landslides plotted at an interval of 50 "hits" of the exceedance threshold.

	75^{th} quantile (mm/day)	**K-S test stat**	**p-value**	**Null rejected**	**alpha**
Central America	6.63	.1792	0.0026	Yes	.997
Himalayan Arc	3.02	.2119	0.0004	Yes	.999
China	2.42	0.0985	0.3776	No	n/a
China – 90^{th} Quantile	5.97	0.2213	0.0553	Yes	.96

Table 1: Test statistics for the 3 study areas, showing the 75^{th} quantile, K-S test statistic and p-value, if the null was rejected, and the confidence level for rejecting the null.